PNAS RESEARCH ARTICLE | NEUROSCIENCE

Thalamocortical axons regulate neurogenesis and laminar fates in the early sensory cortex

Timothy Monko[a,b], Jaclyn Rebertus[a], Jeff Stolley[a], Stephen R. Salton[c], and Yasushi Nakagawa[a,b,d,e,f,1]

Edited by Pasko Rakic, Yale University, New Haven, CT; received January 24, 2022; accepted April 19, 2022

Area-specific axonal projections from the mammalian thalamus shape unique cellular organization in target areas in the adult neocortex. How these axons control neurogenesis and early neuronal fate specification is poorly understood. By using mutant mice lacking the majority of thalamocortical axons, we show that these axons are required for the production and specification of the proper number of layer 4 neurons in primary sensory areas by the neonatal stage. Part of these area-specific roles is played by the thalamus-derived molecule, VGF. Our work reveals that extrinsic cues from sensory thalamic projections have an early role in the formation of cortical cytoarchitecture by enhancing the production and specification of layer 4 neurons.

neocortex | neurogenesis | cell fate | thalamocortical

Significance

This study addresses how the cerebral cortex is partitioned into specialized areas during development. Although both early embryonic patterning and postnatal synaptic input from sensory thalamic nuclei are known to be critical, early roles of thalamic axons in area-specific regulation of cortical neurogenesis are poorly understood. We examined this by developing a genetic mouse model in which thalamocortical projections fail to properly form during embryogenesis, and found these axons are required not only for an enhanced production of superficial layer neurons but also for promoting the layer 4 cell fate, a hallmark of the primary sensory cortex. These findings provide a mechanism by which thalamocortical axons complement the intrinsic programs of neurogenesis and early fate specification.

The adult mammalian nervous system has a remarkable complexity, with thousands of neuronal types, each of which adopts consistent numbers and locations. This fundamental feature critically depends on early developmental mechanisms that control cell divisions and cell fate specification. A unique feature of the nervous system is that neurons can grow axons over great distances and interact with cells far from their cell body. Although such interactions are known to control survival and maturation of the target neurons, they could also influence both the absolute and relative abundances of each neuronal type in the target region. However, we currently have little knowledge on such roles of afferent axonal projections. The mammalian neocortex is composed of diverse types of neurons that are sequentially generated during embryonic development and are arranged in an orderly manner across layers (1–4). In adult neocortex, the distribution and density of each neuronal type differ between areas. Primary (first-order) visual, somatosensory, and auditory areas have a well-developed layer 4 that is directly targeted by axons from corresponding principal sensory nuclei of the thalamus (5, 6). Early patterning mechanisms within the cortex intrinsically confer positional identity of neural progenitor cells and early postmitotic neurons, which leads to the formation of area maps in the postnatal cortex (7–15). These mechanisms influence region-specific regulation of neurogenesis and subsequent specification of neuronal types, which will eventually control the formation of area-specific cytoarchitecture and functional specialization of the neocortex. In contrast, topographic and area-specific projections of thalamocortical axons (TCAs) provide a major extrinsic influence on neocortical cytoarchitecture (7, 16–20). For example, ablation of principal sensory thalamic nuclei or blocking transmitter release from TCA terminals during the postnatal period disrupts anatomical and molecular hallmarks of the primary sensory cortex (21–25). In addition, disrupting the intensity and temporal pattern of spontaneous activity of embryonic thalamic neurons leads to the lack of normal anatomical and functional organization of the primary somatosensory cortex (26). Because TCAs arrive in the cortex during the early period of superficial layer (layers 2 to 4) neurogenesis (Fig. 1 *A* and *B*), production and fate specification of these neurons could be modified by TCAs during embryogenesis. Although eye removal experiments in primates and carnivores suggested the roles of the thalamic input in cortical neurogenesis (27, 28), how TCAs modulate generation and specification of neocortical neurons in an area-specific manner has remained elusive. In mice, deletion of the homeobox gene *Gbx2* prevents most TCAs from reaching the cortex already at mid-embryonic stages (29). However, germline *Gbx2* knockout mice die at birth, precluding the analysis of postnatal brains. In this study, we used thalamus-specific, conditional *Gbx2* knockout mice (30). These mice are postnatally viable, allowing us to examine the requirement of TCAs in cortical development from embryonic to postnatal stages (30, 31, 32). Using these mice, we found evidence indicating that TCAs are required not only to enhance the numbers of progenitor cells but also to promote the layer 4 fate of newly generated superficial layer neurons at the expense of the layer 2/3 fate. This early influence of TCAs, combined with their later roles in activity-dependent neuronal maturation, contributes to the characteristic cytoarchitecture of the primary sensory cortex in the

Author contributions: Y.N. designed research; T.M., J.R., J.S., and Y.N. performed research; T.M., S.R.S., and Y.N. contributed new reagents/analytic tools; T.M., J.R., J.S., and Y.N. analyzed data; and T.M. and Y.N. wrote the paper.

The authors declare no competing interest.

This article is a PNAS Direct Submission.

[1]To whom correspondence may be addressed. Email: nakagawa@umn.edu.

This article contains supporting information online at http://www.pnas.org/lookup/suppl/doi:10.1073/pnas.2201355119/-/DCSupplemental.

Published May 25, 2022.

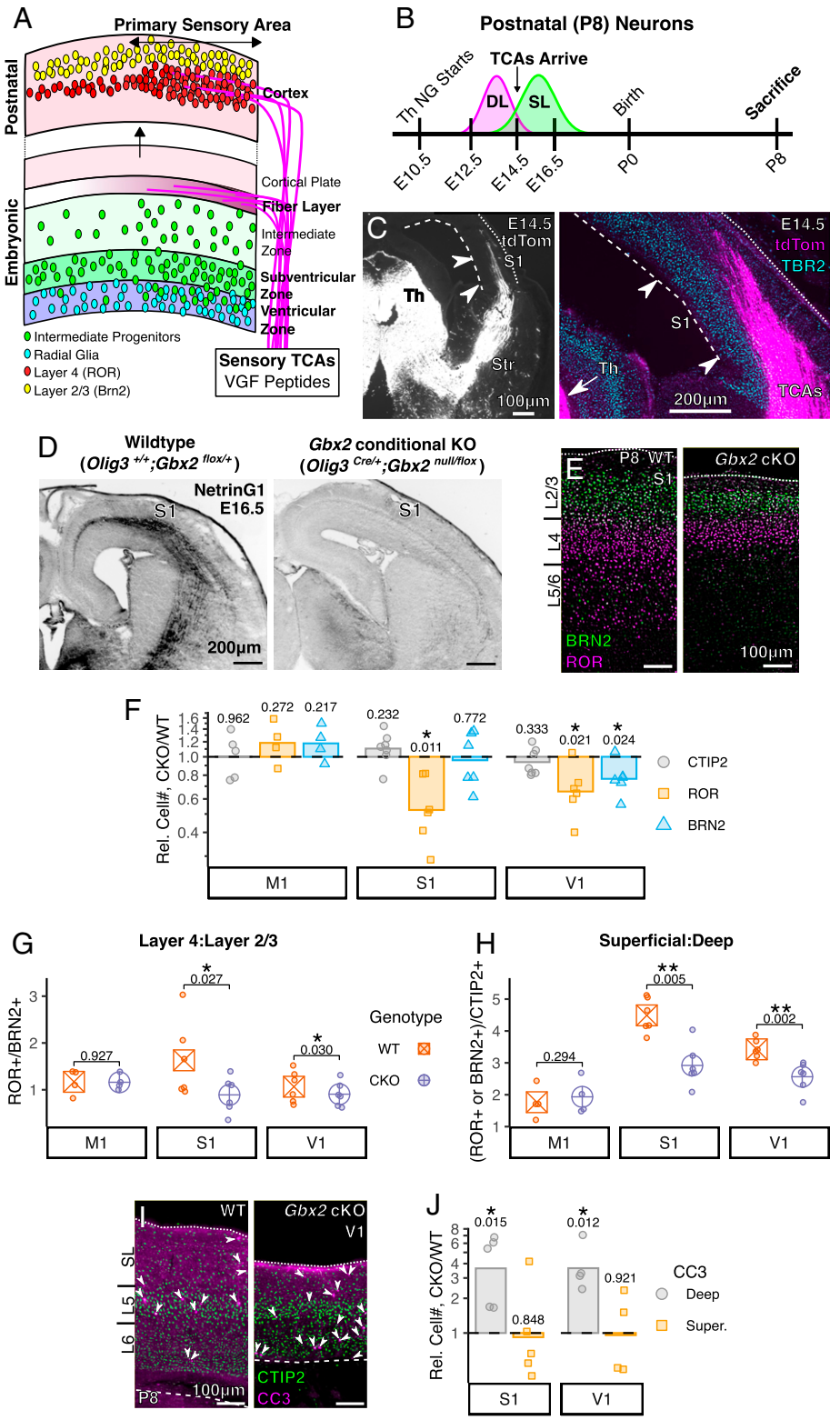

Fig. 1. TCAs increase postnatal neuron number in the primary sensory cortex. (*A*) Schematic summary of our findings; TCAs, including sensory-specific VGF, increase the production of superficial layer neurons and bias their fates toward layer 4. (*B*) Experimental scheme in relation to the timing of neocortical neurogenesis (DL, deep layer; SL, superficial layer) and arrival of TCAs; Th NG, thalamic neurogenesis. (*C*) TCAs (tdTomato driven by *Olig3*^{Cre}) project to the cortex and reside near TBR2^{+} progenitors in the E14.5 S1 cortex. (*D*) Comparison of WT and *Gbx2* cKO TCAs labeled by NetrinG1 (inverted). At E16.5, NetrinG1^{+} TCA axons are found throughout the cortex in WT mice, but, in *Gbx2* cKO mice, few TCAs reach the cortex. (*E*) Layer 4 (ROR^{+}) and layers 2/3 (BRN2^{+}) neurons in the S1 cortex in WT and *Gbx2* cKO mice. (*F*) SL neurons are decreased in both S1 (ROR) and V1 (ROR and BRN2) in *Gbx2* cKO mice; DL (CTIP2) is unchanged. (*G* and *H*) S1 and V1 cortex in *Gbx2* cKO mice have decreased ratios of ROR^{+}-to-BRN2^{+} neurons and SL-to-DL neurons compared with WT controls. (*I*) CTIP2 (DL) and cleaved caspase 3 (CC3: apoptotic cells) in V1 at P8. (*J*) CC3^{+} cells are increased within DLs (bounded by CTIP2^{+} cells) of *Gbx2* cKO mice. Matched ratio *t* test (*F* and *J*) or paired *t* test (*G* and *H*) *P* values are shown between WT and *Gbx2* cKO. For *F* and *J*, data are shown as relative difference of *Gbx2* cKO to WT littermates (dashed line); points represent individual pairs; bar represents pooled mean. Th, thalamus; Str, striatum. **P* < 0.05, ***P* < 0.01.

adult brain. We further provide evidence that the TCA-derived molecule VGF confers sensory-specific regulation of progenitor cell division and neonatal cell fate specification.

Results

TCAs Are Required for the Enhanced Numbers of Superficial Layer Neurons in the Primary Sensory Cortex. By embryonic day 14.5 (E14.5) in mice, TCAs have just reached the prospective somatosensory area and spatially overlap with the domain occupied by intermediate progenitor cells (IPCs) (Fig. 1*C* and *SI Appendix*, Fig. S1*A*) and radial glia (RGs) fibers that span from the ventricular lumen to the pial surface. This timing coincides with the onset of superficial layer neurogenesis in this area (Fig. 1*B*) (33). A vast majority of the prospective visual cortex was not innervated by TCAs at this stage (*SI Appendix*, Fig. S1 *A* and *B*). Newly generated superficial layer neurons in the embryonic neocortex lack patterns of gene expression, morphology, and connectivity that distinguish precise laminar identity in the postnatal brain (34–36). Prospective layer 4 neurons start to show characteristic gene expression by E18.5 (36), and become spatially segregated from layer 2/3 neurons by postnatal day 1 (P1) (34). Between E14.5 and P1, TCAs are in close proximity to both neural progenitor cells and immature neurons (*SI Appendix*, Fig. S1 *C–F*). Therefore, TCAs could interact with these cells and control the generation and/or specification of superficial layer neurons before direct thalamocortical synapses are formed (37, 38). In order to understand the early roles of TCAs, we analyzed mutant mice in which most TCAs fail to project to the cortex, including the primary sensory areas as well as other areas such as primary motor areas and the prefrontal cortex (Fig. 1*D* and *SI Appendix*, Fig. S1*A*) (30, 32). Postnatal viability of *Gbx2* conditional knockout (cKO) mice allowed us to assess the full extent of the TCAs' roles in neocortical development starting at the midembryonic into postnatal stages. At P8, *Gbx2* cKO mice showed a thinning of layer 4 and blurring of the borders of primary sensory areas (*SI Appendix*, Fig. S1*G*) (30). To determine whether neuron numbers are altered in the mutant cortex, we performed immunohistochemistry for transcription factors that are essential for the functional identity of representative classes of excitatory neocortical neurons, including RORα/β (layer 4; with anti-ROR antibody; *SI Appendix*, Fig. S1 *H* and *I*), BRN1/2 (POU3F1/2) [layer 2/3; with anti-BRN2 antibody (39)], and CTIP2 (BCL11B) (layer 5/6) (40–45) (*SI Appendix*, Fig. S1*J*). Among these, RORβ is both necessary and sufficient for the acquisition of characteristic morphology and gene expression patterns of layer 4 spiny stellate neurons (40, 41). We compared the numbers of positive cells between brains of cKO and wild-type (WT) littermates with unbiased threshold-based segmentation, and found that the lack of TCAs in the *Gbx2* cKO cortex results in significantly decreased numbers of ROR-positive (ROR$^+$) layer 4 neurons compared with WT controls in both S1 and visual (V1) areas, but not in M1 (Fig. 1 *E* and *F* and *SI Appendix*, Fig. S1 *K*, *L*, and *O–R*), which normally contains *ROR*β-expressing neurons whose transcriptomic profile is comparable to those in the primary sensory cortex (46, 47). The number of layer 2/3 neurons was also decreased in V1, while layer 5 neurons were not decreased in any of the areas analyzed (Fig. 1*F*). In both S1 and V1 but not in M1, the ratio of layer 4 (ROR$^+$) cells to layer 2/3 (BRN2$^+$) cells was decreased in the cKO cortex (Fig. 1*G*), as was the ratio of superficial (ROR$^+$ and BRN2$^+$) to deep (CTIP2$^+$) layer neurons (Fig. 1*H*). Thus, by P8, TCAs are required to enhance the number of superficial layer neurons as well as the ratio of layer 4 neurons to layer 2/3 neurons in the primary sensory cortex but not in the motor cortex. Because TCAs could provide a survival signal for neurons in their target region, we counted apoptotic cells at P8 and found no increase in cleaved caspase 3 (CC3)-positive cells in superficial layers of *Gbx2* cKO mice (Fig. 1 *I* and *J*). Instead, *Gbx2* cKO mice had increased apoptotic cells in deep layers. This may be due to the decreased corticofugal connectivity (48) and the absence of retrograde survival factors provided by downstream target areas, including the thalamus, in the absence of TCA projections.

TCAs Are Required for Increasing the Number of Progenitor Cells in the Embryonic Sensory Cortex. The above results prompted us to determine whether the decrease in superficial layer neurons in early postnatal *Gbx2* cKO mice is due to their decreased production from progenitor cells during embryogenesis. At E16.5, *Gbx2* cKO mice had reduced numbers of progenitors toward the end of superficial layer neurogenesis (Fig. 2*A*); the number of RGs (PAX6$^+$) was decreased in prospective S1, and IPCs (TBR2$^+$) were also decreased in both prospective S1 and V1, but no changes were observed in prospective M1 and the medial prefrontal cortex (Fig. 2 *B–E* and *SI Appendix*, Fig. S2 *A–D*). The numbers of IPCs or RGs were not decreased in prospective S1, V1, or M1 at E14.5 (Fig. 2*G*) when TCAs have just arrived at prospective S1, but not V1 or M1 (Fig. 2*A* and *SI Appendix*, Fig. S1*B*). Mitotic cells labeled by an antibody against phosphorylated histone H3 (PH3) were decreased at both basal and apical locations at E16.5 in prospective S1 and at the basal location in prospective V1 (Fig. 2 *E* and *F*), but not at E14.5 (Fig. 2*H*). Thus, TCAs are required to increase the number of progenitors and their divisions during the production of superficial layer neurons. To test whether progenitor cells show an increased tendency to exit the cell cycle in the absence of TCAs, which would result in loss of progenitors, we pulse-labeled S-phase cells with 5-ethynyl-2′-deoxyuridine (EdU) 18 h prior to analysis at E16.5 (Fig. 2*I*). We then investigated the short-term fate of daughter cells of the labeled progenitors (49, 50). The numbers of both proliferating (Ki67-positive) and EdU-labeled cells were decreased in both prospective S1 and V1 in *Gbx2* cKO mice (Fig. 2*J*). The rate of cell cycle reentry as measured by the Ki67$^+$EdU$^+$/EdU$^+$ ratio was also decreased (Fig. 2 *K* and *L* and *SI Appendix*, Fig. S2 *E* and *F*). These results collectively demonstrate that, in the primary sensory cortex, TCAs are required for enhancing the number of progenitor cells and prolonging neurogenesis.

Fate Decisions among Superficial Layer Neurons Are Modified by Thalamocortical Projections in the Postnatal Sensory Cortex. A highly distinct cytoarchitectonic feature of the adult primary sensory cortex is the abundance of layer 4 neurons, the main synaptic targets of TCAs derived from corresponding principal sensory nuclei of the thalamus. Synaptic activity of TCAs induces characteristic morphology and patterns of gene expression of layer 4 neurons in postnatal S1 (23–25, 35) and V1 (51). However, the diversification of layer 4 and layer 2/3 fates is first detected perinatally in immature superficial layer neurons, long before morphological features of each neuronal type become evident (34, 36). It is unknown whether this early fate specification is determined strictly by intrinsic gene regulation or is influenced by the thalamic input (2, 3, 52–54). Therefore, we next tested whether TCAs not only are required to enhance the overall number of superficial layer neurons but also affect the early fate choice between layer 2/3 and layer 4

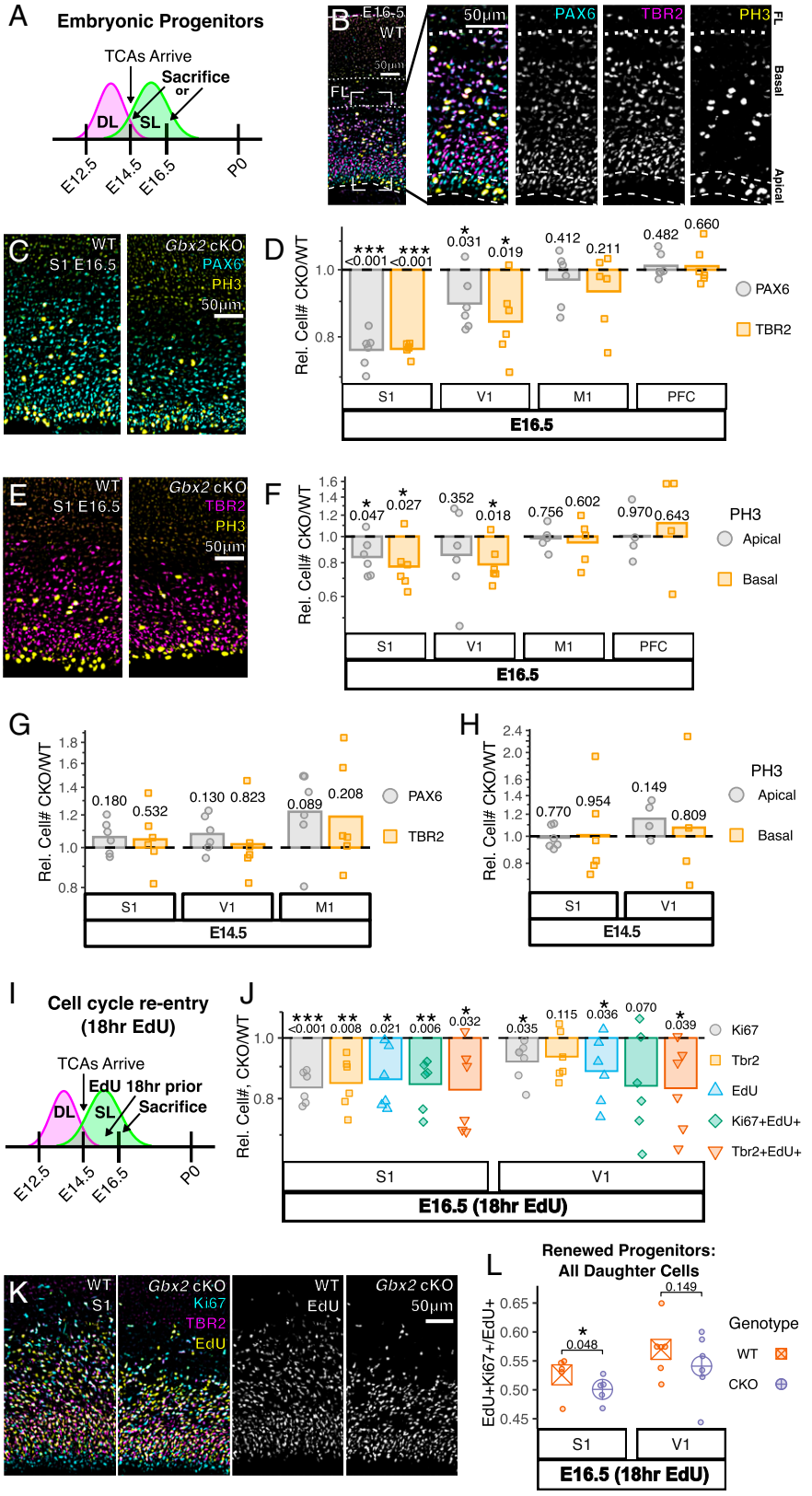

Fig. 2. TCAs increase progenitor numbers, divisions, and cell cycle reentry in the primary sensory cortex. (*A*) Experimental timeline for *B*–*H*. (*B*) At E16.5, the S1 WT cortex progenitors—RGs (PAX6), intermediate progenitors (TBR2), and mitotic cells (PH3)—are below TCAs in the fiber layer (FL); apical PH3 are strictly RGs; basal PH3 are PAX6$^+$ and/or TBR2$^+$. (*C* and *D*) The number of progenitors is decreased in *Gbx2* cKO mice at E16.5 in S1 (TBR2 and PAX6) and V1 (TBR2), but not in the nonsensory cortex M1 (primary motor) or PFC (prefrontal cortex). (*E* and *F*) At E16.5, both apical and basal progenitors divide (PH3$^+$) less in *Gbx2* cKO S1, and basal progenitors divide less in V1. (*G* and *H*) At E14.5 in *Gbx2* cKO mice, neither TBR2 or PAX6 is decreased, and both apical and basal cells also divide (PH3$^+$) similarly in S1 and V1. (*I*) Experimental timeline for *J*–*L*. (*J* and *K*) E16.5 *Gbx2* cKO mice have decreased numbers of progenitors (Ki67$^+$ & TBR2$^+$) and fewer cells proceeding through S-phase (EdU$^+$) in both S1 and V1. (*L*) At E16.5, more progenitors re-enter the cell cycle (EdU$^+$Ki67$^+$) in S1 of WT mice compared with *Gbx2* cKO. Matched ratio *t* test (*D*, *F*, *G*, *H*, and *J*) or paired *t* test (*L*) *P* values are shown between WT and *Gbx2* cKO. For *D*, *F*, *G*, *H*, and *J*, data are shown as relative difference of *Gbx2* cKO to WT littermates (dashed line); points represent individual pairs; bar represents pooled mean. **P* < 0.05, ***P* < 0.01, ****P* < 0.001. See *SI Appendix*, Fig. S2 for breakdown of multichannel images.

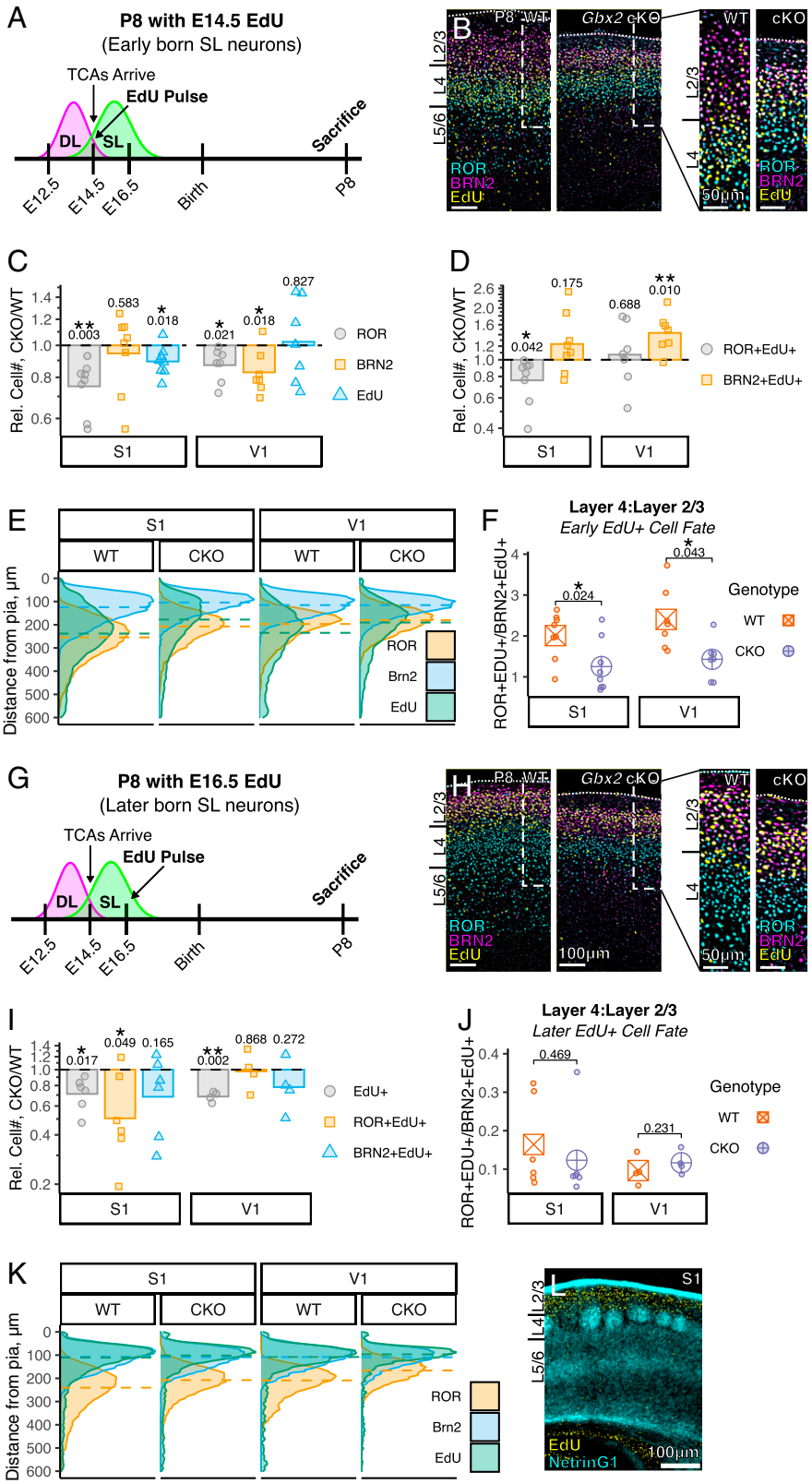

Fig. 3. TCAs bias early-born superficial layer neurons to become layer 4 instead of layer 2/3. (*A*) Experimental timeline for *B*–*F*. (*B*) Distribution of E14.5-labeled EdU$^+$ cells, ROR$^+$ (layer 4) and BRN2$^+$ (layers 2/3) neurons in S1 at P8. *Right* shows high magnification views within the dotted lines on *Left*. (*C*) *Gbx2* cKO reduces EdU in both S1 and V1; EdU-injected WT and *Gbx2* cKO have similar changes to the numbers of SL neurons as in noninjected mice in Fig. 1*F*. (*D*) *Gbx2* cKO reduces ROR$^+$EdU$^+$ cells in S1 and increases Brn2+EdU+ cells in V1. (*E*) EdU$^+$ cells are positioned deeper in S1 and V1 of WT mice compared with *Gbx2* cKO mice. Density curve of distance from pial surface for all cells analyzed in *C*; dashed line is median distance. (*F*) WT EdU-labeled SL neurons are biased toward ROR and against BRN2 when compared with *Gbx2* cKO. (*G*) Experimental timeline for *H*–*L*. (*H*) E16.5-labeled EdU+ cells with SL neuron markers. (*I*) EdU$^+$ cells are reduced in *Gbx2* cKO in both S1 and V1; ROR$^+$EdU$^+$ cells are decreased in S1 *Gbx2* cKO mice. (*J*) E16.5 EdU-labeled neurons are not biased in cell fate by TCAs; note ratio compared to *F*. (*K* and *L*) In S1, E16.5-labeled EdU cells are positioned superficially, mostly above TCA terminals (NetrinG1) that coalesce in "barrels" in layer 4. Matched ratio *t* test (*C*, *D*, and *I*) or paired *t* test (*F* and *J*) *P* values are shown between WT and *Gbx2* cKO. For *C*, *D*, and *I*, data are shown as relative difference of *Gbx2* cKO to WT littermates (dashed line); points represent individual pairs; bar represents pooled mean. **P* < 0.05, ***P* < 0.01, ****P* < 0.001. See *SI Appendix*, Fig. S3 for breakdown of multichannel images.

neurons. For this purpose, we labeled progenitor cells in the S-phase of the cell cycle by EdU at E14.5 or E16.5 (Fig. 3 *A* and *G*), and tracked the fate of neurons that are generated soon after the labeling. We first analyzed each of the cell cohorts at P8 in the primary sensory cortex, when excitatory neurons occupy the final laminar positions but may not have fully developed morphological characteristics (35).

As expected from previous studies (33), the cohort of E14.5-born neurons was mainly found in layer 4 in control S1 (Fig. 3 *B* and *E* and *SI Appendix*, Fig. S3*A*). This cohort of cells shifted superficially toward the BRN2$^+$ layers 2/3 in *Gbx2* cKO mice (Fig. 3 *B* and *E* and *SI Appendix*, Fig. S3*B*), suggesting that postnatal cell position is regulated by TCAs. In S1, the total number of E14.5–EdU$^+$ cells was reduced in the cKO cortex (Fig. 3*C*). Because the number of progenitor cells was not yet reduced at E14.5 (Fig. 2 *G* and *H*), this reduction of E14.5–EdU$^+$ cells indicates that normal proliferation of progenitor cells after E14.5 depends on the projections of TCAs. The number of E14.5-born neurons that have adopted the layer 4 fate (EdU$^+$ROR$^+$) was also decreased, while E14.5-born layer 2/3 neurons (EdU$^+$BRN2$^+$) were not significantly changed (Fig. 3*D*). In V1, although the numbers of EdU$^+$ cells or EdU$^+$ROR$^+$ cells were unchanged, the number of EdU$^+$BRN2$^+$ cells increased in the cKO cortex (Fig. 3 *C* and *D*). In both S1 and V1, the layer 4 to layer 2/3 ratio among the E14.5-born neurons was more than two in the WT cortex (2.03 ± 0.16 for S1, 2.41 ± 0.28 for V1; mean ± SEM), but this ratio was significantly reduced without TCAs (1.39 ± 0.23 for S1, 1.43 ± 0.18 for V1; mean ± SEM) (Fig. 3*F*). Thus, by P8, TCAs are required for the high layer 4 to layer 2/3 ratio in the E14.5-born cohort of neurons in the primary sensory cortex. This result coincides with the reduced ratio of all layer 4 neurons to layer 2/3 neurons regardless of the birth date (Fig. 1*G*).

When progenitor cells were labeled by EdU at E16.5 and the brains were analyzed at P8 (Fig. 3*G*), most EdU$^+$ cells were located in layers 2/3 in both WT and *Gbx2* cKO mice (Fig. 3 *H*, *K*, and *L* and *SI Appendix*, Fig. S3 *C* and *D*). The number of EdU$^+$ cells was decreased in both S1 and V1 of the cKO cortex, and the small number of E16.5-born layer 4 neurons (EdU$^+$ROR$^+$) was further decreased in S1 (Fig. 3*I*). However, the layer 4 to layer 2/3 ratio was unchanged in the cohort of E16.5-born neurons (Fig. 3*J*). Thus, TCAs are required to enhance the production of superficial layer neurons throughout neurogenesis and bias the fate of earlier born neurons toward that of layer 4 instead of layer 2/3.

Early Postmitotic Transition of Laminar Fate Depends on Thalamocortical Input prior to Direct Synapse Formation. We next determined whether sensory TCAs affect the laminar fates of E14.5-born neurons earlier than P8, before the formation of direct synapses between TCAs and prospective layer 4 neurons at around P2 (37, 38). In WT mice at E16.5, EdU$^+$ cells were mostly found in the intermediate zone where IPCs are abundant (Fig. 4*B* and *SI Appendix*, Fig. S4 *B* and *C*), although some EdU$^+$ cells were found more superficially, in the fiber layer overlapping with the incoming TCAs as well as in the cortical plate. Thus, a majority of E14.5-born neurons are still migrating at E16.5 (*SI Appendix*, Fig. S4*A*). At this stage, the upper cortical plate (future superficial layer) contained BRN2$^+$ neurons, while the lower cortical plate (future deep layer) contained CTIP2$^+$ neurons, and expression of ROR was mostly contained within the CTIP2$^+$ layer (Fig. 4*C* and *SI Appendix*, Fig. S4*D*).

By E18.5, many EdU$^+$ cells were found above the fiber layer, mainly within the upper cortical plate overlapping with BRN2 (Fig. 4 *B* and *D* and *SI Appendix*, Fig. S4 *A* and *E–G*). Therefore, a majority of E14.5-born neurons migrate past TCAs between E16.5 and E18.5, potentially allowing them to be influenced by these afferent axons without a direct synaptic input from them. At E18.5, a majority of ROR$^+$ cells were still within the CTIP2$^+$ layer and coexpressed CTIP2 (Fig. 4*C* and *SI Appendix*, Fig. S4 *H* and *I*). The lack of E14.5 EdU labeling in CTIP2$^+$ cells (*SI Appendix*, Fig. S4*I*) suggests that ROR$^+$CTIP2$^+$ cells are future deep-layer neurons, not layer 4 neurons. At this stage, however, ROR was also expressed in a thin layer of cells above the CTIP2$^+$ layer, some of which coexpressed BRN2 (Fig. 4*C* and *SI Appendix*, Fig. S4*H*). This perinatal timing marks the first appearance of layer 4-specific gene expression, which was also detected in single-cell RNA sequencing (36). In prospective S1 of *Gbx2* cKO embryos at E18.5, EdU$^+$ cells were reduced in number compared with WT controls, as were the future superficial layer (EdU$^+$BRN2$^+$) neurons (Fig. 4*H*). However, compared with P8, a much larger proportion of EdU$^+$ cells was positive for BRN2 relative to ROR (compare *SI Appendix*, Figs. S3*E* and S4*J*), and, within the ROR$^+$EdU$^+$ population, nearly half also expressed BRN2 (Fig. 4*J*), revealing E18.5 as a transitory stage for superficial layer neurons to acquire the laminar fate.

Later, at P1, layer 4 and layer 2/3 neurons were separable based on their laminar positions and largely distinct expression of ROR and BRN2, respectively (Fig. 4*E* and *SI Appendix*, Fig. S4*L*), and E14.5-EdU labeled neurons were distributed above layer 5 (CTIP2) neurons (*SI Appendix*, Fig. S4*N*). In the *Gbx2* cKO S1 cortex, the number of E14.5-born, ROR$^+$ cells as well as the layer 4 to layer 2/3 ratio (EdU$^+$ROR$^+$/EdU$^+$BRN2$^+$) was decreased compared with WT littermates (Fig. 4 *I* and *K* and *SI Appendix*, Fig. S4*K*), indicating a shift of molecular laminar fate from layer 4 toward layer 2/3 without TCAs. In addition, the radial positions of EdU-labeled cells were shifted toward the pia at P1 (Fig. 4*G* and *SI Appendix*, Fig. S4 *M–P*). Thus, we conclude that, already at the earliest stage when superficial layer neuron fates are distinguishable between layer 4 and layers 2/3, TCAs are required to promote the fate of layer 4 neurons at the expense of layers 2/3 neurons among E14.5-born superficial layer neurons.

VGF Is a Thalamus-Derived Molecule That Affects Progenitor Cell Division and Layer 4 Fate in the Prenatal and Perinatal Sensory Cortex. The numbers of progenitor cells and layer 4 neurons were decreased in prospective primary sensory areas, but not in the motor area or the medial prefrontal cortex of *Gbx2* cKO mice. Therefore, we predicted that the responsible TCA-derived molecules that influence the number of progenitor cells and laminar fate of immature superficial layer neurons are specifically expressed in principal sensory nuclei of the thalamus, which project axons to primary sensory areas. VGF (nonacronymic) is expressed specifically by nuclei in the thalamus that project to the primary sensory cortex—ventral posterior to S1, dorsal lateral geniculate to V1, and ventral part of the medial geniculate to A1 (55–57). We found that *Vgf* messenger RNA (mRNA) started to be expressed in prospective principal sensory thalamic nuclei as early as at E12.5 and continued throughout development (Fig. 5*B* and *SI Appendix*, Fig. S5*A*). VGF and its cleavage products were present at the terminals of TCAs in the neocortex specific to primary sensory areas (Fig. 5*C* and *SI Appendix*, Fig. S5*B*), and application of uncleaved VGF precursor protein enhanced dendritic growth and survival

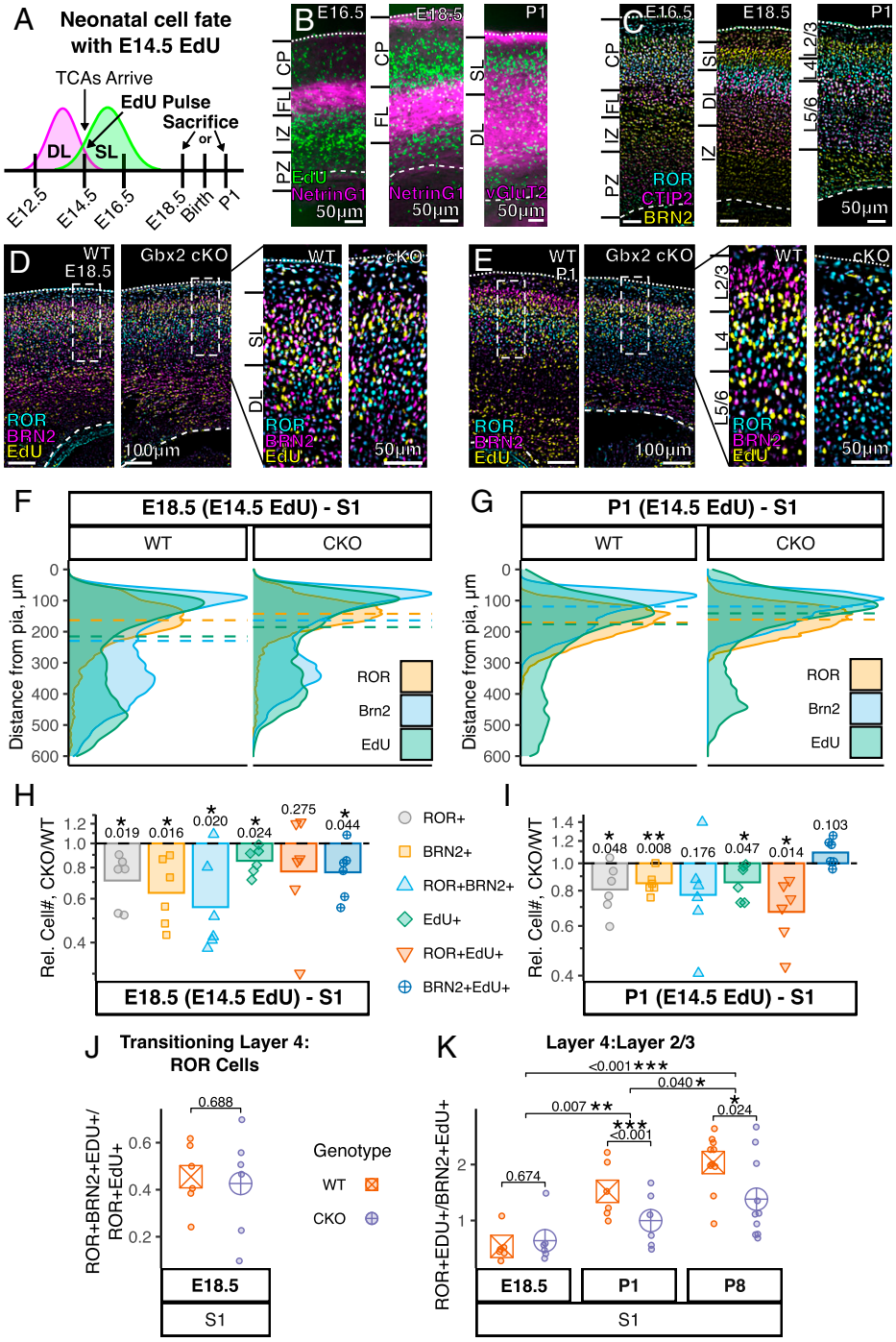

Fig. 4. TCAs regulate the acquisition of cell fate in the perinatal neocortex. (*A*) Experimental timeline; birth, equivalent to E19.5 or P0. (*B*) Positional relationship between the TCAs and cells labeled by EdU at E14.5 (see *SI Appendix*, Fig. S4 *B*, *E*, and *M* for *Gbx2* cKO). At E16.5, labeled cells are mostly below the fiber layer (FL), which contains TCAs (NetrinG1). At E18.5, EdU$^+$ cells are migrating or have migrated through TCAs (NetrinG1). By P1, most labeled cells are in the cortical plate, and TCAs (vGluT2) have grown to future layer 4. (*C*) Dynamic changes of ROR expression. At E16.5, ROR is contained in the CTIP2$^+$ layer. At E18.5, ROR still mostly overlaps CTIP2, but a small fraction of ROR$^+$ cells are first found above layer 5. At P1, ROR$^+$ cells form a more distinctive layer between CTIP$^+$ and BRN2$^+$ layers. (*D* and *E*) Fate analysis of E14.5 EdU-labeled cells analyzed at E18.5 or P1. At E18.5, in both the WT and cKO cortexes, E14.5-labeled EdU$^+$ cells mostly reside above the layer containing ROR and CTIP2, and express BRN2. At P1, a majority of EdU$^+$ cells are in the layer expressing either ROR (layer 4) or BRN2 (layer 2/3). For both *D* and *E*, *Right* shows high magnification views within the dotted lines on *Left*. (*F* and *G*) Distribution of E14.5 EdU-labeled cells in relation to that of ROR$^+$ and BRN2$^+$ cells at E18.5 or P1. At P1, but not at E18.5, EdU$^+$ cells are positioned more superficially in *Gbx2* cKO mice compared with WT littermates. Shown are density curves of distance from pial surface for all cells analyzed in *H* and *I*; dashed line, median distance. (*H*) At E18.5, the number of BRN2$^+$ and ROR$^+$ cells, as well as transitioning ROR$^+$BRN2$^+$ cells, is decreased in *Gbx2* cKO mice; EdU$^+$ and BRN2$^+$EdU$^+$ cells are also decreased. (*I*) At P1, all superficial layer neuron markers (layer 4, ROR; layer 2/3, BRN2), EdU$^+$ cells, and ROR$^+$EdU$^+$ cells are decreased in *Gbx2* cKO mice. (*J*) At E18.5, there is no change in the ratio of E14.5-born transitioning future layer 4 neurons (ROR$^+$BRN2$^+$EdU$^+$) to the total ROR$^+$EdU$^+$ population. (*K*) The ratio of ROR$^+$EdU$^+$ cells over BRN2$^+$EdU$^+$ cells is not significantly changed in *Gbx2* cKO mice at E18.5, but is decreased at P1 and P8. PZ, progenitor zone (including ventricular zone and subventricular zone); IZ, intermediate zone; CP, cortical plate. *P < 0.05, **P < 0.01, ***P < 0.001.

of cortical neurons in vitro (57). Therefore, we tested whether the TCA-derived VGF has a role in progenitor cells and/or immature neurons in the sensory cortex in vivo by analyzing thalamus-specific conditional *Vgf* knockout mice (*Vgf* cKO: *Olig3*$^{Cre/+}$; *Vgf*$^{flox/flox}$), and compared them with WT littermates (*Olig3*$^{+/+}$; *Vgf*$^{flox/(flox\ or\ +)}$ or *Olig3*$^{Cre/+}$; *Vgf*$^{+/+}$). With the

Olig3^{Cre} allele, *Vgf* was specifically deleted in embryonic thalamus (*SI Appendix*, Fig. S5*C*).

At P8, in situ hybridization for *RORβ* mRNA showed thinning of layer 4 in the barrel field of S1 (*SI Appendix*, Fig. S5*D*). With immunohistochemistry combined with the detection of EdU injected at E14.5, we found that the numbers of ROR$^+$ layer 4 neurons in S1 and V1 were reduced in P8 *Vgf* cKO mice (Fig. 5*D*), and the number of E14.5-born layer 4 neurons (EdU$^+$ROR$^+$) was also reduced in V1. However, unlike in *Gbx2* cKO, the total number of E14.5 EdU-labeled cells was unchanged (Fig. 5*D*), suggesting that, for the cohort of E14.5-born neurons, reduction of ROR$^+$ cells was not caused by the reduced overall production of superficial layer neurons. At E16.5, the numbers of both RGs and IPCs were unchanged in *Vgf* cKO mice, although the number of dividing cells (PH3+) cells was reduced in prospective S1 (*SI Appendix*, Fig. S5 *E* and *F*), which indicates that VGF might control the cell cycle length of progenitor cells in the somatosensory cortex. Thus, the lack of TCA-derived VGF accounts for only part of the phenotype seen in the TCA-ablated (*Gbx2* cKO) cortex. At P8, the EdU$^+$ROR$^+$/EdU$^+$BRN2$^+$ ratio was decreased in *Vgf* cKO S1 (Fig. 5*E*) even though, unlike *Gbx2* cKO, E14.5-born cells were not distributed differently among layers 4 (ROR) and 2/3 (BRN2) (Fig. 5*F*), suggesting that the TCA-derived VGF is required to promote the layer 4 fate at the expense of the layer 2/3 fate regardless of the overall cell number or position. We therefore investigated whether VGF, like the TCAs themselves, already affects the fates of superficial layer neurons by neonatal stages. Like at P8, the number of neurons labeled by E14.5 EdU injection was not changed at P1 (Fig. 5*G*), nor was the radial distribution of EdU$^+$ cells different compared with WT littermates (Fig. 5*I*). However, *Vgf* cKO mice had an increased number of E14.5-born neurons that express BRN2 as well as those that express both BRN2 and ROR (Fig. 5*G*). Considering that prospective layer 4 neurons appear to transition from BRN2$^+$ROR$^-$ through BRN2$^+$ROR$^+$ to BRN2$^-$ROR$^+$ during perinatal stages (*SI Appendix*, Fig. S4*A*), the observed changes in the P1 *Vgf* cKO S1 cortex suggest that VGF is required for the timely transition from the transitory, BRN2$^+$ROR$^+$ state to the fully specified layer 4 (BRN2$^-$ROR$^+$) state, likely by suppressing the expression of BRN2. Consistent with this conclusion, we found a decrease in the EdU$^+$BRN2$^-$ROR$^+$/EdU$^+$ROR$^+$ ratio in the cKO brains (Fig. 5*H*).

Discussion

The current study has revealed two distinct roles of TCAs in the early stages of the formation of cytoarchitecture in the primary sensory cortex. First, TCAs are required to enhance neurogenesis during the embryonic stage by increasing the number of progenitor cells that produce superficial layer neurons. In addition, TCAs are required to promote the specification of the layer 4 fate in immature superficial layer neurons at the expense of the layer 2/3 fate by the neonatal stage. These two early roles are consistent with the physical proximity of TCAs to both progenitor cells and immature neurons at the relevant developmental timing before direct synapses are formed between TCAs and layer 4 neurons. Furthermore, we found that the thalamus-derived molecule VGF partially contributes to those roles, implying that multiple molecules derived from thalamic afferents play a role in neurogenesis and fate specification in the early sensory cortex.

Afferent control of neurogenesis in the target region of the developing central nervous system has long been known in the invertebrate visual system, in which retinal axons control cell cycle progression and subsequent differentiation of neurons in their target brain region via the secreted protein Hedgehog (58, 59). In zebrafish, descending projections of diencephalic dopaminergic neurons enhance the production of motor neurons in the spinal cord (60). However, little is known about the direct regulation of neurogenesis by afferent projections in mammalian brains except that olfactory sensory axons modulate the cell-cycle kinetics of olfactory bulb primordium in embryonic telencephalon (61). Protracted neurogenesis in the mammalian neocortex and early projection of TCAs allow close interactions between the afferents and progenitor cells in the embryonic cortex (28). Despite the evidence from eye removal studies in monkeys and ferrets (7, 62–65), direct demonstration of the roles of the TCAs on progenitor cells was lacking. Our current study utilized a mouse model in which few TCAs reach the cortex and found that both RGs and IPCs are reduced in number. In addition, progenitor cells are more likely exit the cell cycle in the absence of normal TCA input in prospective primary sensory areas in the embryonic cortex. Further, we found reduced mitosis of neural progenitor cells in late stages of neurogenesis in mice lacking the TCA-derived protein VGF and its processed neuropeptides. However, lack of VGF did not cause the same extent of defects in neurogenesis observed in mice lacking TCAs, indicating that other thalamus-derived molecules also control the division of cortical progenitor cells.

In the current study, thalamic afferents were found to promote the early specification of layer 4 fate in the primary sensory cortex. Previous studies indicated that ROR*β* and BRN2 have mutually repressive interactions that result in the emergence of gene expression profile and morphological characteristics of layer 4 versus layer 2/3 neurons during perinatal development (34, 40), and that an upstream intrinsic transcriptional network regulates the expression of ROR*β* and BRN2 (52). However, it was unknown whether this early fate specification of immature superficial layer neurons is determined entirely by intrinsic mechanisms or is influenced by the incoming thalamic input in the sensory cortex. Our study demonstrates the requirement of TCAs in this process and the involvement of the thalamus-derived molecule VGF. Our results do not exclude the possibility that TCAs modify the identity of RGs or IPCs in prospective sensory areas so that they have a longer time window and/or a higher likelihood of generating layer 4 neurons as opposed to layer 2/3 neurons. However, a recent single-cell RNA sequencing study showed that newborn superficial layer neurons lack distinct gene expression patterns that separate layer 4 and layer 2/3 fates until the perinatal stage, suggesting that the diversification and identity acquisition of neuronal subpopulations occur postmitotically (36). This is consistent with previous studies (34, 35, 66). Therefore, it is more likely that TCAs bias immature postmitotic neurons to take on the layer 4 fate within the primary sensory cortex. Interestingly, most neurons labeled by EdU injection at E16.5 continued to express BRN2 and migrated to form layers 2/3 in S1 even with TCAs in their vicinity throughout their early development. If TCAs act on postmitotic neurons to influence their fate, how they preferentially bias E14.5-born, but not E16.5-born, neurons to take on the layer 4 fate remains to be elucidated.

Our analysis of conditional *Vgf* knockout mice provides evidence that the thalamus-derived molecule VGF mediates distinct roles of the thalamic axons on neocortical development. A recent study (67) showing that germline deletion of *Vgf* reduces the number of ROR-expressing cells in S1 and V1 at P7 is

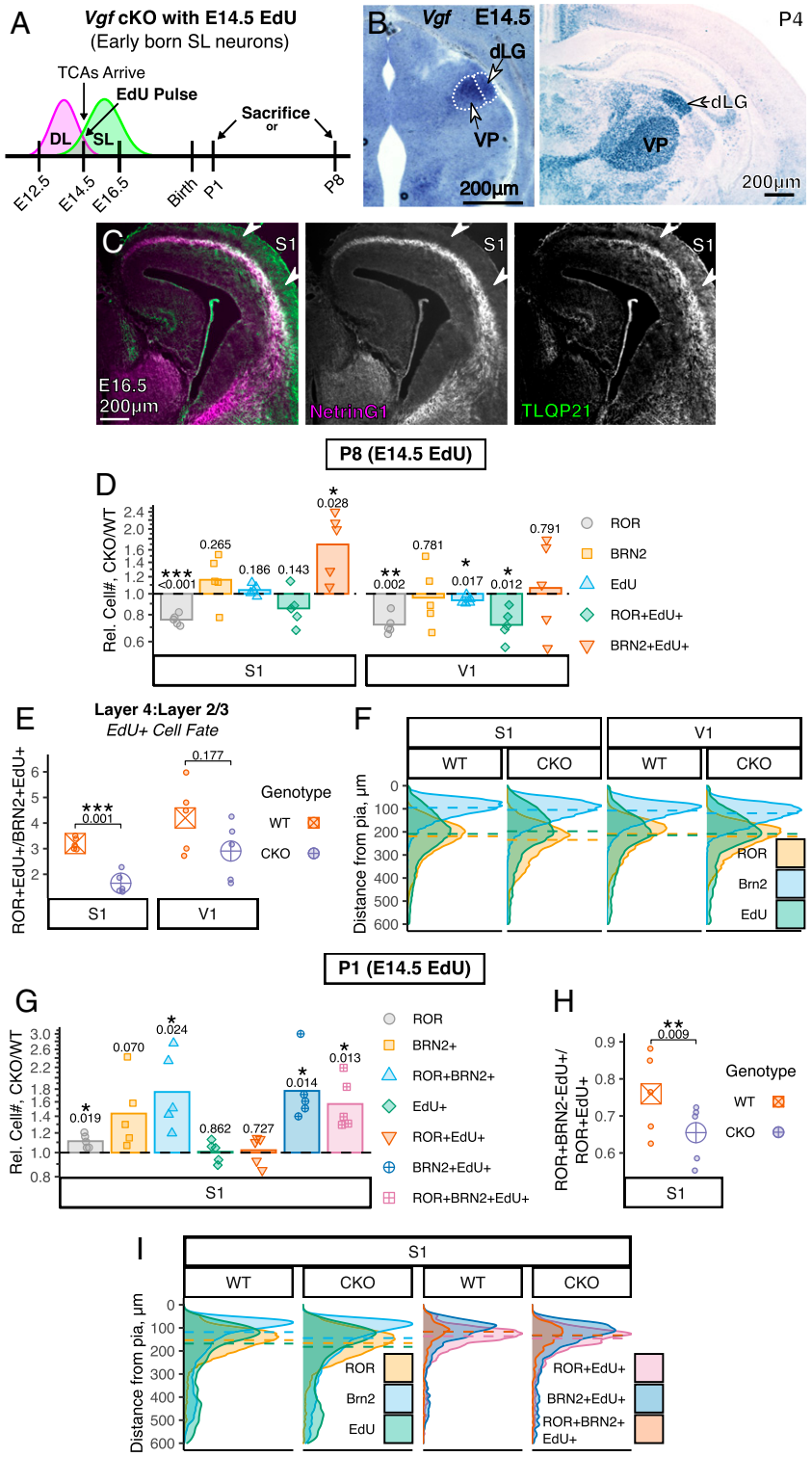

Fig. 5. Thalamus-derived, sensory-specific VGF peptides increase superficial layer neurons and play a role in establishing separate ROR$^+$ and BRN2$^+$ cell populations. (*A*) Experimental timeline. (*B*) In situ hybridization for the *Vgf* mRNA. Principal sensory thalamic nuclei (VP, ventral posterior; dLG, dorsal lateral geniculate) express *Vgf*. High expression of *Vgf* remains isolated to sensory nuclei in the postnatal brain. (*C*) At E16.5, TCAs (NetrinG1) contain high levels of a VGF peptide, TLQP21, in future sensory areas (S1). (*D*) At P8, *Vgf* cKO mice injected with EdU at E14.5 have reduced numbers of layer 4 ROR$^+$ neurons in both S1 and V1 compared with WT mice. EdU is slightly decreased in V1 of *Vgf* cKO mice. *Vgf* cKO mice have more Brn2$^+$EdU$^+$ cells in S1 and fewer ROR$^+$EdU$^+$ cells in V1. (*E*) VGF biases E14.5-born neurons to become layer 4 (ROR$^+$) compared to layers 2/3 (BRN2$^+$) in S1, with a trend toward this ratio in V1. (*F*) Radial distribution of E14.5 EdU$^+$ cells is not different between WT and *Vgf* cKO mice at P8. Shown are density curves of distance from pial surface for all cells analyzed in *D*; dashed line, median distance. (*G*) At P1, *Vgf* cKO mice have increased ROR$^+$, BRN2$^+$, and ROR$^+$BRN2$^+$ cells as well as more BRN2$^+$EdU$^+$ and ROR$^+$BRN2$^+$EdU$^+$ cells after EdU injection at E14.5. (*H*) At P1, *Vgf* cKO mice have fewer E14.5-born (EdU$^+$) ROR$^+$ neurons that transition to fully specified layer 4 (ROR$^+$BRN2$^-$) neurons. (*I*) At P1, EdU, ROR, and BRN2 distribution is not different between WT and *Vgf* cKO mice. More ROR$^+$BRN2$^+$EdU$^+$ cells are present in *Vgf* cKO mice, and the increased overlap of ROR$^+$EdU$^+$ and BRN2$^+$EdU$^+$ cells is likely to account for this. Shown are density curves of distance from pial surface for all cells analyzed in *G*; dashed line, median distance. Matched ratio *t* test (*D* and *G*) or paired *t* test (*E* and *H*) *P* values shown are between WT and *Gbx2* cKO. For *D* and *G*, data are shown as relative difference of *Gbx2* cKO to WT littermates (dashed line); points represent individual pairs; bar represents pooled mean. **P* < 0.05, ***P* < 0.01, ****P* < 0.001. See *SI Appendix*, Fig. S5 for breakdown of multichannel images.

consistent with our results on thalamus-specific *Vgf* deletion. The VGF precursor protein is cleaved into at least a dozen biologically active peptides (56), and little is known about the roles of individual VGF peptides in neural development. One candidate is the C-terminal VGF peptide TLQP-62, which controls hippocampal neurogenesis (68) as well as depression (69) and nerve injury-induced hypersensitivity (70), although the identity of its receptor is currently unknown. Another C-terminal peptide, TLQP-21 (71, 72), is localized in TCAs (Fig. 5*C*) and modulates microglial function through its receptors C3aR1 (73–76) and C1qBP (77). Thus, these peptides might have direct or indirect effects on newborn neurons or progenitor cells during embryogenesis and early postnatal cortical development.

In summary, our present study provides a mechanism by which afferent input from the thalamus complements the intrinsic program in early cortical development, allowing the sequential generation of diverse neuronal types in an area-specific manner. Further studies are expected to reveal the spatially and temporally regulated molecular interplay between the thalamic input and cortical cells across different areas.

Materials and Methods

Detailed descriptions for all procedures are available in *SI Appendix*.

Mice. Care and experimentation on mice were done in accordance with the Institutional Animal Care and Use Committee at the University of Minnesota. Noon of the day on which the vaginal plug was found was counted as embryonic day 0.5 (E0.5), and the day of birth (E19.5) was designated as P0. To generate mice with a conditional deletion of TCAs, $Olig3^{Cre/+}$; $Gbx2^{null/+}$ mice were bred with $Gbx2^{flox/flox}$ mice as in ref. 30. $Gbx2^{flox/flox}$ mice (78) were obtained from Jackson Laboratory. $Olig3^{+/+}$; $Gbx2^{flox/+}$ were used as WT littermates and compared to $Olig3^{Cre/+}$; $Gbx2^{null/flox}$ as *Gbx2* cKO mice. Mice were kept in C57BL/6 background, and embryos or pups of either sex were used. Possibly due to the continued outbreeding of both $Olig3^{Cre/+}$ and $Gbx2^{flox/flox}$ mice for the maintenance of the colony, the lateral ventricles were enlarged in *Gbx2* cKO mice used in this study in varying degrees in comparison with the same mutants reported in our previous study (30). Representative images are shown in *SI Appendix*, Fig. S1*G*. This morphological change became noticeable at P1 and became more severe at later postnatal stages. However, the postnatal phenotypes including the altered layer 4/layer 2–3 ratio are not explainable simply due to the altered structure. Mice were matched within littermates of WT and cKO to control for small differences between litters; therefore, litters without both a cKO and a WT pup were not analyzed. Mice with a conditional deletion of *Vgf* from TCAs were generated by breeding $Olig3^{Cre/+}$;$Vgf^{flox/+}$ mice with $Vgf^{flox/flox}$ or $Vgf^{flox/+}$ mice (79). $Olig3^{+/+}$; $Vgf^{flox/(flox\ or\ +)}$ or $Olig3^{Cre/+}$; $Vgf^{+/+}$ were used as WT littermates and compared with $Olig3^{Cre/+}$; $Vgf^{flox/flox}$ as *Vgf* cKO mice. *Vgf* cKO mice were kept in C57BL/6 background, pups of either sex were used, and mice were matched littermates for comparison between cKO and WT.

EdU Incorporation. For 5-ethynyl-2′-deoxyuridine (EdU, Carbosynth) incorporation experiments, mice were administered 50 μg of EdU per g body weight dissolved in saline via intraperitoneal injection.

In Situ Hybridization and Immunohistochemical Staining. In situ hybridization using digoxigenin-labeled probes and immunohistochemical staining were performed based on ref. 80.

Imaging. For cell counting, images of sections that underwent immunohistochemistry were taken using an E800 upright microscope (Nikon) with a Retiga EXi camera (Qimaging) or Zeiss Axio Observer Z1 motorized microscope controlled by ZEN software (2.6) with a QuantEM:512SC camera (Photometrics). Images were taken with either Open Lab software (Improvision) or Micromanager (81).

Binning. Images were entirely processed within the FIJI (Fiji is just ImageJ) distribution of ImageJ (82). With Open-Lab Images, individual TIFF files for each channel were opened and combined into a composite stack (see code/software: ref. 83). Then, a rectangular region of interest was overlaid onto the image from pial surface to ventricle and at a width of either 200 μm (embryonic nonsensory cortex) or 400 μm (embryonic sensory cortex and postnatal cortex). Images acquired with Micromanager were opened, and the bin was overlaid (84). Detailed methods for placing bins are described in *SI Appendix*.

Thresholding. Images were processed with a custom ImageJ macro, which would batch process all images with identical parameters across paired littermates (85).

Colocalization. To determine double- and triple-positive cells, an optional section within the thresholding batch macro or a separate batch macro (86) was utilized.

Experimental Design and Statistical Analyses. Littermates were matched for experiments and analysis between *Gbx2* cKO or *Vgf* cKO and WT mice to control for immunohistochemical variability between pairs; WT mice are the control.

Code/Software.
FIJI. The FIJI package based on ImageJ2 was utilized for all processing of image data directly from the microscope (82, 87). Custom FIJI macros were written using the ImageJ Macro scripting language and are available on a GitHub repository (88).

Data Availability. Custom FIJI macros were written using the ImageJ Macro scripting language and are available on a GitHub repository: https://github.com/TimMonko/NeurogenesisThalamocorticalPaper/ (88) . All other study data are included in the article and/or *SI Appendix*.

ACKNOWLEDGMENTS. We thank Grace Heimdahl, Ethan Chase, Earl Parker Scott, Thomas Bao, Emma Breyak, Ellie Wheeler, and Xiangyu Zou for technical assistance; Kate Neitzke, Armando Thull, Patrick Willey, and University Imaging Center (University of Minnesota) for help with imaging; Matt Simon, Lynn Wang, Alicia Cowles, Troy Liu, Yuria Shimizu, Samantha Dabruzzi, and Peter Goncharov for contribution to the early phase of the study; Marija Cvetanovic, Zhe Chen, Linda McLoon, and Steven McLoon for critical reading of the manuscript; Lucy Vulchanova for anti-TLQP-21 antibody; and Henk Stunnenberg for anti-RORβ antibody. This work was supported by NIH Grants T32 GM113846 and NIH T32 EY025187 to T.M. and NIH Grants R21 NS117978 and R01 NS049357 to Y.N., Winston and Maxim Wallin Neuroscience Discovery Fund, Whitehall Foundation and University of Minnesota.

Author affiliations: [a]Department of Neuroscience, University of Minnesota Medical School, Minneapolis, MN 55455; [b]Graduate Program in Neuroscience, University of Minnesota Medical School, Minneapolis, MN 55455; [c]Nash Family Department of Neuroscience, Friedman Brain Institute, Icahn School of Medicine at Mount Sinai, New York, NY 10029; [d]Developmental Biology Center, University of Minnesota, Minneapolis, MN 55455; [e]Masonic Institute for the Developing Brain, University of Minnesota, Minneapolis, MN 55455; and [f]Stem Cell Institute, University of Minnesota Medical School, Minneapolis, MN 55455

1. S. K. McConnell, The determination of neuronal fate in the cerebral cortex. *Trends Neurosci.* **12**, 342–349 (1989).
2. A. Llorca *et al.*, A stochastic framework of neurogenesis underlies the assembly of neocortical cytoarchitecture. *eLife* **8**, e51381 (2019).
3. P. Gao *et al.*, Deterministic progenitor behavior and unitary production of neurons in the neocortex. *Cell* **159**, 775–788 (2014).
4. P. Oberst *et al.*, Temporal plasticity of apical progenitors in the developing mouse neocortex. *Nature* **573**, 370–374 (2019).
5. A. Peters, E. G. Jones, *Cerebral Cortex: Cellular Components of the Cerebral Cortex* (Springer, 1984).
6. K. Brodmann, *Vergleichende Lokalisationslehre der Grosshirnrinde* [in German] (Johann Ambrosius Barth, Leipzig, Germany, 1909).
7. P. Rakic, Specification of cerebral cortical areas. *Science* **241**, 170–176 (1988).
8. T. Fukuchi-Shimogori, E. A. Grove, Neocortex patterning by the secreted signaling molecule FGF8. *Science* **294**, 1071–1074 (2001).
9. T. Fukuchi-Shimogori, E. A. Grove, Emx2 patterns the neocortex by regulating FGF positional signaling. *Nat. Neurosci.* **6**, 825–831 (2003).
10. K. M. Bishop, G. Goudreau, D. D. O'Leary, Regulation of area identity in the mammalian neocortex by Emx2 and Pax6. *Science* **288**, 344–349 (2000).
11. J. A. Cholfin, J. L. Rubenstein, Patterning of frontal cortex subdivisions by Fgf17. *Proc. Natl. Acad. Sci. U.S.A.* **104**, 7652–7657 (2007).
12. G. E. Elsen *et al.*, The protomap is propagated to cortical plate neurons through an Eomes-ependent intermediate map. *Proc. Natl. Acad. Sci. U.S.A.* **110**, 4081–4086 (2013).

13. K. Pattabiraman *et al.*, Transcriptional regulation of enhancers active in protodomains of the developing cerebral cortex. *Neuron* **82**, 989–1003 (2014).
14. S. Garel, K. J. Huffman, J. L. Rubenstein, Molecular regionalization of the neocortex is disrupted in Fgf8 hypomorphic mutants. *Development* **130**, 1903–1914 (2003).
15. O. Golonzhka *et al.*, Pbx regulates patterning of the cerebral cortex in progenitors and postmitotic neurons. *Neuron* **88**, 1192–1207 (2015).
16. G. López-Bendito, Development of the thalamocortical interactions: Past, present and future. *Neuroscience* **385**, 67–74 (2018).
17. D. D. O'Leary, Do cortical areas emerge from a protocortex? *Trends Neurosci.* **12**, 400–406 (1989).
18. C. R. Cadwell, A. Bhaduri, M. A. Mostajo-Radji, M. G. Keefe, T. J. Nowakowski, Development and arealization of the cerebral cortex. *Neuron* **103**, 980–1004 (2019).
19. Y. Nakagawa, Development of the thalamus: From early patterning to regulation of cortical functions. *Wiley Interdiscip. Rev. Dev. Biol.* **8**, e345 (2019).
20. U. Borello, H. Kennedy, C. Dehay, The logistics of afferent cortical specification in mice and men. *Semin. Cell Dev. Biol.* **76**, 112–119 (2018).
21. S. P. Wise, E. G. Jones, Developmental studies of thalamocortical and commissural connections in the rat somatic sensory cortex. *J. Comp. Neurol.* **178**, 187–208 (1978).
22. S. J. Chou *et al.*, Geniculocortical input drives genetic distinctions between primary and higher-order visual areas. *Science* **340**, 1239–1242 (2013).
23. G. Pouchelon *et al.*, Modality-specific thalamocortical inputs instruct the identity of postsynaptic L4 neurons. *Nature* **511**, 471–474 (2014).
24. N. Narboux-Nême *et al.*, Neurotransmitter release at the thalamocortical synapse instructs barrel formation but not axon patterning in the somatosensory cortex. *J. Neurosci.* **32**, 6183–6196 (2012).
25. H. Li *et al.*, Laminar and columnar development of barrel cortex relies on thalamocortical neurotransmission. *Neuron* **79**, 970–986 (2013).
26. N. Antón-Bolaños *et al.*, Prenatal activity from thalamic neurons governs the emergence of functional cortical maps in mice. *Science* **364**, 987–990 (2019).
27. C. Dehay, G. Horsburgh, M. Berland, H. Killackey, H. Kennedy, The effects of bilateral enucleation in the primate fetus on the parcellation of visual cortex. *Brain Res. Dev. Brain Res.* **62**, 137–141 (1991).
28. I. Reillo *et al.*, A complex code of extrinsic influences on cortical progenitor cells of higher mammals. *Cereb. Cortex* **27**, 4586–4606 (2017).
29. E. M. Miyashita-Lin, R. Hevner, K. M. Wassarman, S. Martinez, J. L. Rubenstein, Early neocortical regionalization in the absence of thalamic innervation. *Science* **285**, 906–909 (1999).
30. T. Y. Vue *et al.*, Thalamic control of neocortical area formation in mice. *J. Neurosci.* **33**, 8442–8453 (2013).
31. S. Zechel, Y. Nakagawa, C. F. Ibáñez, Thalamo-cortical axons regulate the radial dispersion of neocortical GABAergic interneurons. *eLife* **5**, e20770 (2016).
32. R. Larsen, A. Proue, E. P. Scott, M. Christiansen, Y. Nakagawa, The thalamus regulates retinoic acid signaling and development of parvalbumin interneurons in postnatal mouse prefrontal cortex. *eNeuro* **6**, ENEURO.0018-19.2019 (2019).
33. E. Klingler *et al.*, A translaminar genetic logic for the circuit identity of intracortically projecting neurons. *Curr. Biol.* **29**, 332–339.e5 (2019).
34. K. Oishi, M. Aramaki, K. Nakajima, Mutually repressive interaction between Brn1/2 and Rorb contributes to the establishment of neocortical layer 2/3 and layer 4. *Proc. Natl. Acad. Sci. U.S.A.* **113**, 3371–3376 (2016).
35. N. S. De León Reyes *et al.*, Transient callosal projections of L4 neurons are eliminated for the acquisition of local connectivity. *Nat. Commun.* **10**, 4549 (2019).
36. D. J. Di Bella *et al.*, Molecular logic of cellular diversification in the mouse cerebral cortex. *Nature* **595**, 554–559 (2021).
37. A. Agmon, G. Hollrigel, D. K. O'Dowd, Functional GABAergic synaptic connection in neonatal mouse barrel cortex. *J. Neurosci.* **16**, 4684–4695 (1996).
38. Z. Molnár, T. Kurotani, S. Higashi, N. Yamamoto, K. Toyama, Development of functional thalamocortical synapses studied with current source-density analysis in whole forebrain slices in the rat. *Brain Res. Bull.* **60**, 355–371 (2003).
39. T. Yamanaka *et al.*, Mutant huntingtin fragment selectively suppresses Brn-2 POU domain transcription factor to mediate hypothalamic cell dysfunction. *Hum. Mol. Genet.* **19**, 2099–2112 (2010).
40. E. A. Clark *et al.*, Cortical RORβ is required for layer 4 transcriptional identity and barrel integrity. *eLife* **9**, e52370 (2020).
41. D. J. Jabaudon, S. J. Shnider, D. J. Tischfield, M. Galazo, J. D. Macklis, ROR{beta} induces barrel-like neuronal clusters in the developing neocortex. *Cereb. Cortex* **22**, 996–1006 (2012).
42. M. H. Dominguez, A. E. Ayoub, P. Rakic, POU-III transcription factors (Brn1, Brn2, and Oct6) influence neurogenesis, molecular identity, and migratory destination of upper-layer cells of the cerebral cortex. *Cereb. Cortex* **23**, 2632–2643 (2013).
43. Y. Sugitani *et al.*, Brn-1 and Brn-2 share crucial roles in the production and positioning of mouse neocortical neurons. *Genes Dev.* **16**, 1760–1765 (2002).
44. P. Arlotta *et al.*, Neuronal subtype-specific genes that control corticospinal motor neuron development in vivo. *Neuron* **45**, 207–221 (2005).
45. B. Chen *et al.*, The Fezf2-Ctip2 genetic pathway regulates the fate choice of subcortical projection neurons in the developing cerebral cortex. *Proc. Natl. Acad. Sci. U.S.A.* **105**, 11382–11387 (2008).
46. N. Schaeren-Wiemers, E. André, J. P. Kapfhammer, M. Becker-André, The expression pattern of the orphan nuclear receptor RORbeta in the developing and adult rat nervous system suggests a role in the processing of sensory information and in circadian rhythm. *Eur. J. Neurosci.* **9**, 2687–2701 (1997).
47. Z. Yao *et al.*, A transcriptomic and epigenomic cell atlas of the mouse primary motor cortex. *Nature* **598**, 103–110 (2021).
48. R. F. Hevner, E. Miyashita-Lin, J. L. Rubenstein, Cortical and thalamic axon pathfinding defects in Tbr1, Gbx2, and Pax6 mutant mice: Evidence that cortical and thalamic axons interact and guide each other. *J. Comp. Neurol.* **447**, 8–17 (2002).
49. T. Takahashi, R. S. Nowakowski, V. S. Caviness Jr., Early ontogeny of the secondary proliferative population of the embryonic murine cerebral wall. *J. Neurosci.* **15**, 6058–6068 (1995).
50. L. Wang, K. K. Bluske, L. K. Dickel, Y. Nakagawa, Basal progenitor cells in the embryonic mouse thalamus - Their molecular characterization and the role of neurogenins and Pax6. *Neural Dev.* **6**, 35 (2011).
51. E. M. Callaway, V. Borrell, Developmental sculpting of dendritic morphology of layer 4 neurons in visual cortex: Influence of retinal input. *J. Neurosci.* **31**, 7456–7470 (2011).
52. P. S. Hou, G. Miyoshi, C. Hanashima, Sensory cortex wiring requires preselection of short- and long-range projection neurons through an Egr-Foxg1-COUP-TFI network. *Nat. Commun.* **10**, 3581 (2019).
53. E. Klingler, D. Jabaudon, Do progenitors play dice? *eLife* **9**, e54042 (2020).
54. A. Llorca, O. Marín, Orchestrated freedom: New insights into cortical neurogenesis. *Curr. Opin. Neurobiol.* **66**, 48–56 (2021).
55. S. E. Snyder, J. E. Pintar, S. R. Salton, Developmental expression of VGF mRNA in the prenatal and postnatal rat. *J. Comp. Neurol.* **394**, 64–90 (1998).
56. A. Bartolomucci *et al.*, The extended granin family: Structure, function, and biomedical implications. *Endocr. Rev.* **32**, 755–797 (2011).
57. H. Sato *et al.*, Thalamus-derived molecules promote survival and dendritic growth of developing cortical neurons. *J. Neurosci.* **32**, 15388–15402 (2012).
58. S. B. Selleck, C. Gonzalez, D. M. Glover, K. White, Regulation of the G1-S transition in postembryonic neuronal precursors by axon ingrowth. *Nature* **355**, 253–255 (1992).
59. Z. Huang, S. Kunes, Hedgehog, transmitted along retinal axons, triggers neurogenesis in the developing visual centers of the Drosophila brain. *Cell* **86**, 411–422 (1996).
60. M. M. Reimer *et al.*, Dopamine from the brain promotes spinal motor neuron generation during development and adult regeneration. *Dev. Cell* **25**, 478–491 (2013).
61. Q. Gong, M. T. Shipley, Evidence that pioneer olfactory axons regulate telencephalon cell cycle kinetics to induce the formation of the olfactory bulb. *Neuron* **14**, 91–101 (1995).
62. C. Dehay, G. Horsburgh, M. Berland, H. Killackey, H. Kennedy, Maturation and connectivity of the visual cortex in monkey is altered by prenatal removal of retinal input. *Nature* **337**, 265–267 (1989).
63. P. Rakic, I. Suñer, R. W. Williams, A novel cytoarchitectonic area induced experimentally within the primate visual cortex. *Proc. Natl. Acad. Sci. U.S.A.* **88**, 2083–2087 (1991).
64. C. Dehay, P. Giroud, M. Berland, H. Killackey, H. Kennedy, Contribution of thalamic input to the specification of cytoarchitectonic cortical fields in the primate: Effects of bilateral enucleation in the fetal monkey on the boundaries, dimensions, and gyrification of striate and extrastriate cortex. *J. Comp. Neurol.* **367**, 70–89 (1996).
65. I. Reillo, C. de Juan Romero, M. A. García-Cabezas, V. Borrell, A role for intermediate radial glia in the tangential expansion of the mammalian cerebral cortex. *Cereb. Cortex* **21**, 1674–1694 (2011).
66. S. Yoshinaga *et al.*, Comprehensive characterization of migration profiles of murine cerebral cortical neurons during development using FlashTag labeling. *iScience* **24**, 102277 (2021).
67. H. Sato *et al.*, Thalamocortical axons control the cytoarchitecture of neocortical layers by area-specific supply of VGF. *eLife* **11**, e67549 (2022).
68. S. Thakker-Varia *et al.*, VGF (TLQP-62)-induced neurogenesis targets early phase neural progenitor cells in the adult hippocampus and requires glutamate and BDNF signaling. *Stem Cell Res. (Amst.)* **12**, 762–777 (2014).
69. C. Jiang *et al.*, VGF function in depression and antidepressant efficacy. *Mol. Psychiatry* **23**, 1632–1642 (2018).
70. A. G. J. Skorput *et al.*, Involvement of the VGF-derived peptide TLQP-62 in nerve injury-induced hypersensitivity and spinal neuroplasticity. *Pain* **159**, 1802–1813 (2018).
71. A. Bartolomucci *et al.*, TLQP-21, a VGF-derived peptide, increases energy expenditure and prevents the early phase of diet-induced obesity. *Proc. Natl. Acad. Sci. U.S.A.* **103**, 14584–14589 (2006).
72. M. S. Riedl *et al.*, Proteomic analysis uncovers novel actions of the neurosecretory protein VGF in nociceptive processing. *J. Neurosci.* **29**, 13377–13388 (2009).
73. S. Hannedouche *et al.*, Identification of the C3a receptor (C3AR1) as the target of the VGF-derived peptide TLQP-21 in rodent cells. *J. Biol. Chem.* **288**, 27434–27443 (2013).
74. C. Cero *et al.*, The TLQP-21 peptide activates the G-protein-coupled receptor C3aR1 via a folding-upon-binding mechanism. *Structure* **22**, 1744–1753 (2014).
75. S. Doolen *et al.*, Complement 3a receptor in dorsal horn microglia mediates pronociceptive neuropeptide signaling. *Glia* **65**, 1976–1989 (2017).
76. F. El Gaamouch *et al.*, VGF-derived peptide TLQP-21 modulates microglial function through C3aR1 signaling pathways and reduces neuropathology in 5xFAD mice. *Mol. Neurodegener.* **15**, 4 (2020).
77. N. Elmadany *et al.*, The VGF-derived peptide TLQP21 impairs purinergic control of chemotaxis and phagocytosis in mouse microglia. *J. Neurosci.* **40**, 3320–3331 (2020).
78. J. Y. Li, Z. Lao, A. L. Joyner, Changing requirements for Gbx2 in development of the cerebellum and maintenance of the mid/hindbrain organizer. *Neuron* **36**, 31–43 (2002).
79. W. J. Lin *et al.*, VGF and its C-terminal peptide TLQP-62 regulate memory formation in hippocampus via a BDNF-TrkB-dependent mechanism. *J. Neurosci.* **35**, 10343–10356 (2015).
80. T. Y. Vue *et al.*, Characterization of progenitor domains in the developing mouse thalamus. *J. Comp. Neurol.* **505**, 73–91 (2007).
81. A. D. Edelstein *et al.*, Advanced methods of microscope control using μManager software. *J. Biol. Methods* **1**, e10 (2014).
82. J. Schindelin *et al.*, Fiji: An open-source platform for biological-image analysis. *Nat. Methods* **9**, 676–682 (2012).
83. T. Monko *et al.*, FIJI_BinningMacro_OpenLab.ijm. GitHub. https://github.com/TimMonko/NeurogenesisThalamocorticalPaper/blob/1bd8c49a85bd784d29a3ad5b2d82dfe8fb38b490/FIJI%20-%20Defunct%20Macros/FIJI_BinningMacro_OpenLab.ijm. Deposited 16 June 2021.
84. T. Monko *et al.*, FIJI_BinningMacro_MicroManager.ijm. GitHub. https://github.com/TimMonko/NeurogenesisThalamocorticalPaper/blob/1bd8c49a85bd784d29a3ad5b2d82dfe8fb38b490/FIJI%20-%20Current%20Macros/FIJI_BinningMacro_MicroManager.ijm. Deposited 16 June 2021.
85. T. Monko *et al.*, FIJI_Thresholding_WatershedSegmentation.ijm. https://github.com/TimMonko/NeurogenesisThalamocorticalPaper/blob/1bd8c49a85bd784d29a3ad5b2d82dfe8fb38b490/FIJI%20-%20Current%20Macros/FIJI_Thresholding_WatershedSegmentation.ijm. Deposited 16 June 2021.
86. T. Monko *et al.*, FIJI_Coloc_Subtractor.ijm. GitHub. https://github.com/TimMonko/NeurogenesisThalamocorticalPaper/blob/1bd8c49a85bd784d29a3ad5b2d82dfe8fb38b490/FIJI%20-%20Current%20Macros/FIJI_Coloc_Subtractor.ijm. Deposited 16 June 2021.
87. C. T. Rueden *et al.*, ImageJ2: ImageJ for the next generation of scientific image data. *BMC Bioinformatics* **18**, 529 (2017).
88. T. Monko *et al.*, NeurogenesisThalamocorticalPaper. GitHub. https://github.com/TimMonko/NeurogenesisThalamocorticalPaper/. Deposited 5 July 2021.